Supplementary Material

Motion Deblurring from a Single Image using Circular Sensor Motion

Yosuke Bando[†,§], Bing-Yu Chen[‡], and Tomoyuki Nishita[§]

[†]TOSHIBA Corporation
[§]The University of Tokyo
[‡]National Taiwan University

Abstract

This document presents supplementary results, data, and derivations that are not included in the paper due to space limitation. The sections, equations, and figures in this supplementary material are not numbered from 1 in order to prevent confusion with those in the paper.

8. Additional Results

This section shows some additional results.

8.1. Example of a License Plate

Fig. 20 shows an example of a license plate of a motorbike. The digits and characters are legible in the deblurred image in Fig. 20(c). The motorbike is identified as moving rightward (not leftward), which is unavailable information from the static camera image in Fig. 20(a). This information may be useful for traffic accident investigation (e.g., to identify whether the motorbike crashed into another car on the left or it was trying to avoid being hit by that car).

(a) (b) (c)

Figure 20: *License plate of a motorbike. (a) From a static camera. (b) From the circular motion camera. (c) Deblurring result of (b).*

8.2. Additional Recognizability Comparisons

In Fig. 15 we demonstrated that the facial feature point detection succeeded for a circular motion camera image even before deconvolution, while it failed for a static camera image. To compare with the other image capture strategies, we used high speed camera images similarly to the resolution chart examples in Fig. 16. Examples of a vertically moving face are shown in Fig. 21. The facial feature point detection succeeded only for the circular motion camera image of Fig. 21(d), as shown in Fig. 21(e).

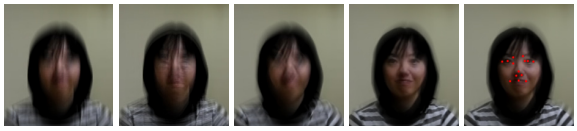

(a) (b) (c) (d) (e)

Figure 21: *Motion-blurred face simulated from high speed camera images. (a) Static camera. (b) Coded exposure camera. (c) Motion-invariant camera. (d) Circular motion camera. (e) Facial feature point detection succeeded for the circular motion camera image (d) without deconvolution (and failed for the others (a-c)).*

[†] yosuke1.bando@toshiba.co.jp
[‡] robin@ntu.edu.tw
[§] {ybando, nis}@nis-lab.is.s.u-tokyo.ac.jp

Table 1: *Result statistics of the paired-comparison for subjective evaluation of image recognizability.*

Object motion	Static object				Horizontal object motion				Oblique object motion				Vertical object motion			
Camera motion	Sta	Cod	Mot	Cir	Sta	Cod	Mot	Cir	Sta	Cod	Mot	Cir	Sta	Cod	Mot	Cir
Static camera	—	0.448	0.006	0.000	—	0.897	0.982	0.964	—	0.885	0.964	1.000	—	0.897	0.248	0.988
Coded exposure	0.552	—	0.000	0.006	0.103	—	0.927	0.970	0.115	—	0.545	0.994	0.103	—	0.079	0.933
Motion-invariant	0.994	1.000	—	0.000	0.018	0.073	—	0.606	0.036	0.455	—	1.000	0.752	0.921	—	0.988
Circular (ours)	1.000	0.994	1.000	—	0.036	0.030	0.394	—	0.000	0.006	0.000	—	0.012	0.067	0.012	—

Sta: static camera, Cod: coded exposure camera, Mot: motion-invariant camera, Cir: circular motion camera.

Fig. 22 shows examples of a license plate. They are also simulated from high speed camera images (note that Fig. 20 is a real example, not a simulated one). Large digits "72-14" are legible for all of the capture strategies, but the characters above these digits are hard to recognize in the static and coded exposure images shown in Figs. 22(a,b). Legibility for the motion invariant camera image (c) is not as good as that for the circular motion camera image (d) as the motion direction is slightly off the horizontal.

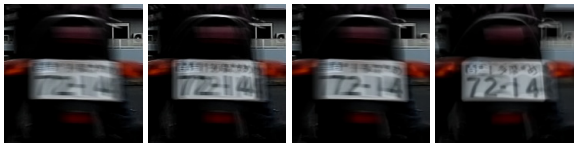

(a) (b) (c) (d)

Figure 22: *Motion-blurred license plate simulated from high speed camera images. (a) Static camera. (b) Coded exposure camera. (c) Motion-invariant camera. (d) Circular motion camera.*

8.3. Simple Workaround for Static Scene Parts

As mentioned in the paper, one of the drawbacks of our method is that it blurs and degrades static scene parts. Since it is often possible to take another photograph of static scene parts before or after the fact, we can use it as a background image as shown in Fig. 23.

Figure 23: *The deconvolved background in Fig. 14(c) was replaced by another image captured without moving the sensor.*

9. Statistics of the Subjective Evaluation

In Sec. 6 we described the subjective evaluation of recognizability. The results of the paired-comparison test prior to being processed by Thurstone's method are summarized in Table 1. For example, "0.552" at the leftmost column means that, for static objects, 55.2% of the subjects preferred the images captured with a static camera over those with the coded exposure camera.

10. More Revolutions of the Sensor

In Fig. 4(1) we showed that circularly moving the sensor twice with different speeds within a single exposure does not fill in the frequency zeros of the motion blur PSFs. Even if we increase the number of revolutions, frequency zeros will not disappear as shown in Fig. 24. Moreover, PSFs become more like the ones resulting from a static camera or the coded exposure camera, and begin to favor static objects.

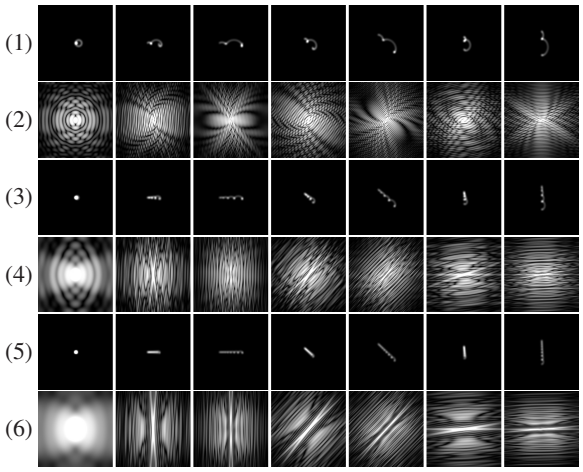

(1) (2) (3) (4) (5) (6)

(a) (b) (c) (d) (e) (f) (g)

Figure 24: *Motion blur PSFs and their corresponding log power spectra. Rows: (1) PSFs and (2) power spectra resulting from two-revolution circular sensor motion (same as Fig. 4(1)). (3)(4) Five-revolution. (5)(6) Ten-revolution. Columns: (a) Static object. (b)(c) Horizontal object motion at different speeds. (d)(e) Oblique object motion. (f)(g) Vertical object motion.*

11. Derivations

For completeness, here we include derivations relevant to Sec. 4 in the paper which we omitted for brevity.

11.1. Non-existence of 2D Motion-invariant Camera

For 2D linear object motion, we can show that motion-invariance is not achievable.

Proposition 1: *There is no sensor motion that makes PSF invariant to 2D linear object motion.*

Proof: Suppose there exists such sensor motion $\mathbf{m}(t) = (m_x(t), m_y(t))$. As it is invariant to 2D linear object motion, for any constant object velocity $\mathbf{v} = (s_x, s_y)$, there must exist c and $\mathbf{d}$ such that

$$\mathbf{m}(t) - \mathbf{v}t = \mathbf{m}(t+c) + \mathbf{d}, \tag{10}$$

which means that the object motion only translates the sensor motion path $\mathbf{m}(t)$. Differentiating Eq. (10) and rearranging, we have:

$$\frac{d\mathbf{m}(t+c)}{dt} - \frac{d\mathbf{m}(t)}{dt} = -\mathbf{v}. \tag{11}$$

From this equation we can see that $d\mathbf{m}(t)/dt$ is a linear function of t. Letting $dm_x(t)/dt = a_x t + b_x$ and $dm_y(t)/dt = a_y t + b_y$, and plugging them back into Eq. (11), we obtain:

$$\begin{aligned} a_x c &= -s_x, \\ a_y c &= -s_y, \end{aligned} \tag{12}$$

and c exists only when $-s_x/a_x = -s_y/a_y$, leading to a contradiction. □

11.2. The Slicing Relationship

In Sec. 4.1 we used the property that the 2D Fourier transform of a motion blur PSF for object velocity $\mathbf{v}$ is a 2D slice of the 3D Fourier transform $\hat{p}(\mathbf{f}, f_t)$ (Eq. (2)) of a camera path in the xyt space-time, where the slice is taken along the plane of $f_t = -\mathbf{v}\cdot\mathbf{f}$. This relationship can be derived as follows.

As we are interested in motion blur PSF, we consider an object as a point light source moving at velocity $\mathbf{v}$ as $\delta(\mathbf{x} - \mathbf{v}t)$. An image of this object (i.e., PSF) observed from a camera moving according to $\mathbf{m}(t)$ during exposure time $[-T, +T]$ is given as:

$$h(\mathbf{x}) = \int_{-T}^{+T} \delta(\mathbf{x} - \mathbf{v}t + \mathbf{m}(t))dt. \tag{13}$$

Taking its 2D Fourier transform leads to:

$$\hat{h}(\mathbf{f}) = \int_{\Omega}\int_{-T}^{+T} \delta(\mathbf{x} - \mathbf{v}t + \mathbf{m}(t)) e^{-2\pi i \mathbf{f}\cdot\mathbf{x}} dt d\mathbf{x}, \tag{14}$$

which can be integrated with respect to $\mathbf{x}$ to yield:

$$\hat{h}(\mathbf{f}) = \int_{-T}^{+T} e^{-2\pi i \mathbf{f}\cdot(-\mathbf{m}(t)+\mathbf{v}t)} dt. \tag{15}$$

Meanwhile, by integrating Eq. (2) with respect to $\mathbf{x}$, we obtain:

$$\hat{p}(\mathbf{f}, f_t) = \int_{-T}^{+T} e^{-2\pi i(\mathbf{f}\cdot\mathbf{m}(t) + f_t t)} dt. \tag{16}$$

Comparing Eqs. (15) and (16), we see that $\hat{h}(\mathbf{f}) = \hat{p}(-\mathbf{f}, \mathbf{f}\cdot\mathbf{v})$, meaning that the Fourier transform of a motion blur PSF is a 2D slice of $\hat{p}(\mathbf{f}, f_t)$ along the plane of $f_t = -\mathbf{v}\cdot\mathbf{f}$.

11.3. The Amount of Frequency Budget

Here we show that the frequency budget for the 3D Fourier transform $\hat{p}(\mathbf{f}, f_t)$ of a camera path is exactly $2T$ along each vertical line $\mathbf{f} = \mathbf{c}$ (the line shown in red and green in Fig. 5(a)) for any given spatial frequency $\mathbf{c}$: i.e., $\int |\hat{p}(\mathbf{c}, f_t)|^2 df_t = 2T$, as described in Sec. 4.1.

From Eq. (16), we see that $\hat{p}(\mathbf{c}, f_t)$, when viewed as a function of f_t, is the (1D) Fourier transform of the following function:

$$b(t) = \begin{cases} e^{-2\pi i \mathbf{c}\cdot\mathbf{m}(t)} & \text{for } t \in [-T, +T] \\ 0 & \text{otherwise} \end{cases}. \tag{17}$$

Therefore, using the Parseval's theorem,

$$\begin{aligned} \int_{-\infty}^{+\infty} |\hat{p}(\mathbf{c}, f_t)|^2 df_t &= \int_{-\infty}^{+\infty} |b(t)|^2 dt \\ &= \int_{-T}^{+T} 1\, dt = 2T. \end{aligned} \tag{18}$$

11.4. Asymptotic Form of Bessel Functions

To derive Eq. (6) in Sec. 4.2, we used the asymptotic form of Bessel functions $J_k(z)$. The specific formula is as follows.

$$J_k(z) \approx \sqrt{\frac{2}{\pi z}} \cos\left(z - \frac{k\pi}{2} - \frac{\pi}{4}\right), \tag{19}$$

which is valid for $z \gg k^2$.